Doping-induced phase transitions in ferroelectric $BaTiO_3$ from first-principles calculations

Yoshiki Iwazaki,[1,2,*] Toshimasa Suzuki,[1] Youichi Mizuno,[1] and Shinji Tsuneyuki[2]
[1]*Taiyo Yuden Co., Ltd., 5607-2 Nakamuroda-machi Takasaki-shi, Gunma 370-3347, Japan*
[2]*Department of Physics, University of Tokyo, 7-3-1 Hongo Bunkyo-ku, Tokyo 113-0033, Japan*
(Received 27 September 2011; revised manuscript received 25 June 2012; published 5 December 2012)

Carrier-electron-induced phase transition from tetragonal to cubic phases in $BaTiO_3$ is studied using first-principles calculation. Our results show that the disappearance of the ferroelectric phase is an intrinsic effect resulting from carrier electron doping in $BaTiO_3$. We further clarify that the lattice disorder induced by donor dopants such as oxygen vacancies and substitutionally doped Nb^{5+} at Ti^{4+} sites accelerates the disappearance of the tetragonal phase in $BaTiO_3$.

DOI: 10.1103/PhysRevB.86.214103 PACS number(s): 77.80.B−, 61.72.Bb, 71.15.Mb

I. INTRODUCTION

Owing to the simplicity of its crystal structure, perovskite-type $BaTiO_3$ has been one of the most extensively studied ferroelectric materials since its discovery more than 60 years ago. $BaTiO_3$ exhibits a series of phase transitions from paraelectric cubic (C) to ferroelectric tetragonal (T), orthorhombic (O), and rhombohedral (R) phases at 396, 278, and 183 K, respectively. Ferroelectricity in $BaTiO_3$ can be easily eliminated by introduction of defects and impurities,[1–5] application of pressure or stress,[6–8] or by the surface effects in thin films and fine particles.[9–12] The disappearance of ferroelectricity in $BaTiO_3$ is of great importance for not only device applications but also understanding the origin of ferroelectricity. Recent studies of carrier electron doping by substituting Nb^{5+} at Ti^{4+} sites, La^{3+} at Ba^{2+} sites,[3–5] and by introducing oxygen vacancies (V_O^{2+})[1,2,13] showed that metallic conductivity appears in $BaTiO_3$ above the critical electron concentration $n \approx 1 \times 10^{20}$ cm^{-3}. One would expect that the ferroelectric phase would disappear in the presence of metallic conductivity because of the screening of the long-range electrostatic interactions that are responsible for the emergence of ferroelectricity.[14,15] However, experiments with reduced $BaTiO_{3-\delta}$ indicate that the presence of itinerant electrons does not immediately suppress the ferroelectric phase, but ferroelectric distortion is sustained even under metallic conductivity.[1,2] Under metallic conductivity, ferroelectric hysteresis loops cannot be measured because of large leakage currents, but phase transition can be confirmed by structural changes measured by x-ray diffraction, dc and optical conductivities,[1,2] and characteristic volume shrinkage that occurs at phase transitions from low- to high-temperature phases.[16] Recent experiments with $BaTiO_{3-\delta}$ samples predicted disappearance of ferroelectric phases at the critical electron concentration $n \approx 1.9 \times 10^{21}$ cm^{-3}.[1] Although many previous experiments suggested that donor-type doping leads to the disappearance of ferroelectric phases,[1–5,13,16] it is not clear whether the transition from ferroelectric to paraelectric phases is caused by the introduction of free-carrier electrons or by the lattice disorder induced by the donor dopants; this is because these two effects are very difficult to separate experimentally.[1,16] Therefore, it is highly desirable to form a theoretical basis to understand this subject. In this paper we present the results of our first-principles calculation of the carrier-electron-induced ferroelectric to paraelectric phase transition in $BaTiO_3$. Our results show that the disappearance of the ferroelectric phase is an intrinsic effect caused by carrier electron doping in $BaTiO_3$ and that the lattice disorder caused by donor dopants accelerates the transition from low- to high-symmetry phases.

II. COMPUTATIONAL DETAILS

The calculations are based on density functional theory (DFT) with the ultrasoft pseudopotential (USP) implemented in the CASTEP code.[17] The atomic reference configurations used in the construction of USPs are $5s^25p^66s^2$ for Ba, $3s^23p^63d^24s^2$ for Ti, $4s^24p^64d^45s^1$ for Nb, and $2s^22p^4$ for O. A Plane-wave basis set with a cutoff energy of 500 eV was used in all calculations. Special k-point sampling with $8 \times 8 \times 8$ grids was selected for unit cell calculations and the grids were reduced in sequential supercell calculations while maintaining the same accuracy. The local density approximation was adopted in all calculations, and cell parameters were relaxed under isobaric conditions with a convergence tolerance of 10 MPa. Our calculations gave $c/a = 1.010$ (Expt. 1.011) and volume $v = 61.40$ Å^3 (Expt. 64.32 Å^3) in T phase $BaTiO_3$, which agrees well with previous reports.[18,19] The effects of electron doping and dopant-induced lattice disorder were evaluated using different charge compensation models; namely, charge compensation with uniform background charges without the effects of lattice disorder and compensation with supercell models containing typical dopants such as Nb^{5+} at Ti^{4+} sites and V_O^{2+}.

III. RESULTS

A. Electron-induced phase transition

Figure 1(a) shows the crystal structure of the T phase $BaTiO_3$ unit cell with $P4mm$ symmetry. The electron-induced changes in the inner fractional atomic coordinates and the tetragonality (c/a ratio) of the T phase $BaTiO_3$ are shown in Figs. 1(b) and 1(c), respectively. The tetragonality decreases with increasing electron doping and the crystal structure becomes cubic at a critical electron concentration of $n_{\text{elec.}} = 0.105\ e$/(unit cell) ($1.68 \times 10^{21}$ cm^{-3}). It should be noted that the ferroelectric displacement is remarkably depend on k-point sampling grids. Even though the c/a ratio is well converged with $8 \times 8 \times 8$ grids in insulating $BaTiO_3$, the c/a ratio in electron doped system further decreases by increasing the

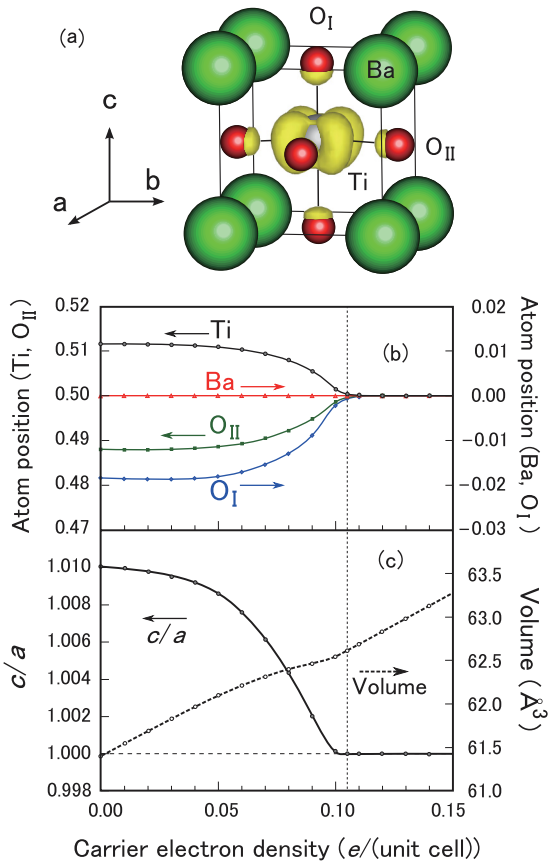

FIG. 1. (Color online) (a) $BaTiO_3$ tetragonal crystal structure and doped-electron distribution of 0.1 e/(unit cell). (b) Shifts of c-axis atomic positions of Ba, Ti, O_I, and O_{II} in the $BaTiO_3$ unit cell induced by electron doping. (c) The c/a ratio and unit cell volume of $BaTiO_3$ as a function of carrier electron doping.

number of the grids. As a result, the critical electron concentration for T-C phase transition slightly reduces and converges into 0.085 e/(unit cell) (1.36×10^{21} cm^{-3}) with $14 \times 14 \times 14$ k-point grids. In these calculations, overall charge neutrality is maintained by uniform background charges; hence, the results shown in Fig. 1 are due to carrier electrons and no lattice disorder is induced by donor dopants. The volume of electron-doped $BaTiO_3$ monotonically increases with an increase in the electron concentration, as shown in Fig. 1(c), with a slight anomaly occurring at the electron concentration at which carrier-induced phase transition occurs. The electron doping calculations for O and R phases result in a paraelectric phase transition with almost the same critical electron concentration for T phase, which indicate that the disappearance of the ferroelectric phase is an intrinsic result of electron doping in $BaTiO_3$.

We now discuss the role of the carrier electrons doped into ferroelectric $BaTiO_3$ on the basis of previous explanations for the emergence of ferroelectricity. Previous studies indicate that the hybridization of Ti-3d and O-2p is crucial for the ferroelectricity in $BaTiO_3$, and the ferroelectric instability vanishes if 3d variational freedom is removed.[14,15] The p-d hybridization is also reported to be greatly changed when the ferroelectric atomic displacements are emphasized.[20] However, we confirmed that the difference in the hybridization between T and

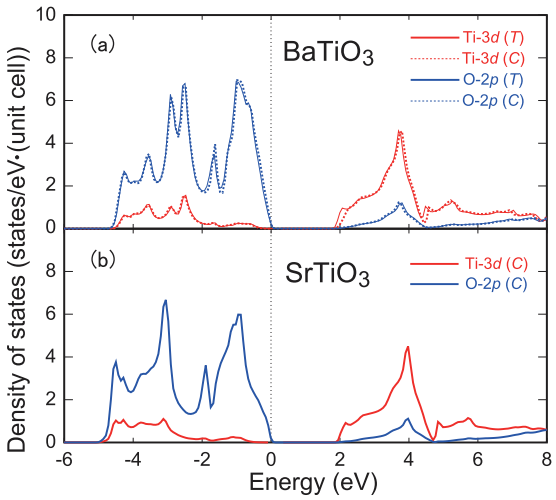

FIG. 2. (Color online) Partial density of states of (a) Ti-3d and O-2p in T and C phases of $BaTiO_3$ and (b) C phase $SrTiO_3$ in charge neutral condition. The lattice constant and inner-atomic coordinates of crystal structures are optimized. In both figures, O-2p states are the sum of contributions from all oxygen atoms in the unit cell.

C phases of $BaTiO_3$ is very small when we optimized both the lattice constant and inner-atomic coordinates, as shown in Fig. 2(a). The same feature is preserved under electron doping, and it is therefore very unclear whether the change in the p-d hybridization is responsible for the electron-induced cubic phase transition. A similar problem has been pointed out for the difference between $SrTiO_3$ and $BaTiO_3$.[21] $SrTiO_3$ is a typical paraelectric perovskite-type oxide that differs from $BaTiO_3$ only in the size of the alkaline-earth A-site ion and the p-d hybridizations in both materials are very similar, as shown in Figs. 2(a) and 2(b). Consequently, some explanation other than the effect of the hybridization would be required for the electron induced T-C phase transition.

The well known alternative explanation for the ferroelectric lattice instability is ratio of ionic radii that comprise the perovskite lattice,[21–23] which is conventionally described by the tolerance factor $t_{ATiO_3} = (r_A + r_O)/\sqrt{2}(r_{Ti} + r_O)$, where r_A, r_{Ti}, and r_O are the ionic radii of A-site, Ti, and O ions in $ATiO_3$, respectively.[21–25] In fact, the tolerance factor t is quite effective in predicting the global trend of lattice instabilities in perovskites, such as ferroelectric distortions[21,23] and tilts and rotations of BO_6 octahedra[22,23] including antiferrodistortive (AFD) instabilities of $SrTiO_3$.[24,25] The lattice of perovskites with $t > 1$ is generally too large for the B-site Ti cation, and the Ti ion tends to displace,[23] as observed in $BaTiO_3$ that has $t = 1.06$ with Shannon's ionic radii; on the other hand, $SrTiO_3$ with $t = 1$ favors the densely packed C phase. Figure 1(a) shows the distribution of carrier electrons doped into T phase $BaTiO_3$. The figure indicates that the carrier electrons are mainly distributed over the Ti-3d orbital with weak hybridization on the O-2p orbital, reflecting the characteristic of the conduction-band bottom of $BaTiO_3$ shown in Fig. 2(a). The carrier distribution indicates that the introduced electrons mainly reduce the valence of the Ti ions, which leads to a selective increase in r_{Ti}. Therefore, one qualitative interpretation for the carrier-induced phase

transition in $BaTiO_3$ would be that the decrease in t is caused by the increase in r_{Ti}.

A more quantitative discussion is possible on the basis of nonempirical model calculation, which indicates that long-range Coulomb energy favors ferroelectric distortion, whereas shot-range repulsions stabilize the cubic phase.[14] In addition, note that the cubic phase obtained by carrier electron doping is an ideal system for investigating the origin of the ferroelectric lattice instability in $BaTiO_3$. This is because the difference between the cubic (electron doped) and tetragonal (undoped) systems is only a slight difference in electron number, which enables us to study very small energy gains caused by the ferroelectric lattice deformation. The DFT total energy E_{total} can be divided into two parts:

$$E_{\text{total}} = E_{\text{kinetic}} + E_{\text{Coulomb}}, \tag{1}$$

$$E_{\text{kinetic}} = \sum_{n\mathbf{k}} \langle \phi_{n\mathbf{k}} | -\frac{1}{2}\Delta | \phi_{n\mathbf{k}} \rangle, \tag{2}$$

$$E_{\text{Coulomb}} = E_{\text{Hartree}} + E_{\text{xc}} + E_{\text{ext}} + E_{\text{Ewald}}, \tag{3}$$

where E_{kinetic} is kinetic energy denoted by Eq. (2) and E_{Coulomb} is Coulomb energy composed of Hartree (E_{Hartree}), exchange-correlation (E_{xc}), external (E_{ext}), and Ewald (E_{Ewald}) energies, as shown by Eq. (3). We calculated the ferroelectric deformation potential ΔE_{total}, which is the energy gain due to soft-mode distortion,[15] and evaluate the contributions of the kinetic ($\Delta E_{\text{kinetic}}$) and Coulomb ($\Delta E_{\text{Coulomb}}$) energies to ΔE_{total}.[26] The results, shown in Fig. 3(a), indicate that the local minimum in ΔE_{total}, which induces ferroelectric deformation, arises from the stronger energy gain in $\Delta E_{\text{Coulomb}}$ compared with that in $\Delta E_{\text{kinetic}}$. The results show that the Coulomb energy favors the ferroelectric deformation in $BaTiO_3$, as expected from previous model calculations.[14] The potential depth of ΔE_{total} at the local minimum is about two orders of magnitude smaller than the variations in $\Delta E_{\text{Coulomb}}$ or $\Delta E_{\text{kinetic}}$, which indicates that the ferroelectric deformation is based on a very delicate balance between these two contributions to the total energy.

When electrons are introduced into the lattice, the local minimum in ΔE_{total} disappears, as shown in Fig. 3(a) (dashed line); that is, a cubic phase transition occurs. To investigate the contribution of the kinetic and Coulomb energies to the disappearance of the local minimum in ΔE_{total}, we divide the total energy difference $\delta E_{\text{total}} = \Delta E_{\text{total (charged)}} - \Delta E_{\text{total (neutral)}}$ into Coulomb ($\delta E_{\text{Coulomb}}$) and kinetic ($\delta E_{\text{kinetic}}$) parts and individually evaluate each contribution to δE_{total}. The results [Fig. 3(b)] indicate that electron doping mainly increases $\delta E_{\text{Coulomb}}$, which implies that screening of the Coulomb energy induced by carrier electrons contributes crucially to the disappearance of the ferroelectric lattice instability. The sharp increase in the kinetic energy around Ti position 0.525 would be related to the minimum distance allowed between ions, which is typically called Pauli repulsion. These results strongly suggest that the ferroelectric phase of $BaTiO_3$ is stabilized by the Coulomb energy and that electron doping weakens the stabilization by screening the contribution of the Coulomb energy, which results in the disappearance of the ferroelectric phase in $BaTiO_3$.

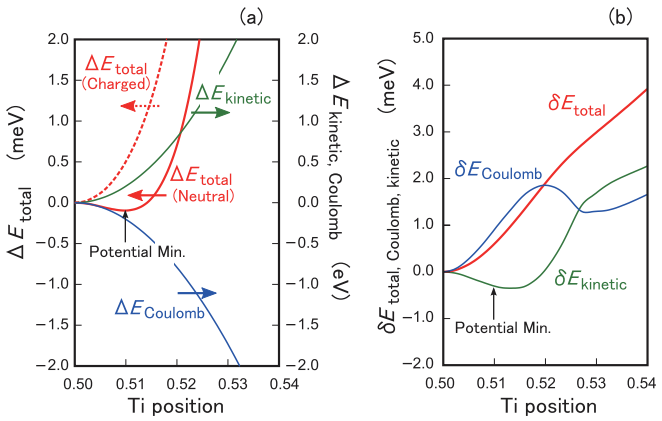

FIG. 3. (Color online) (a) Total energy difference $\Delta E_{\text{total (Neutral)}}$ (the deformation potential) as a function of soft-mode distortion in neutral $BaTiO_3$. Kinetic and Coulomb ($\Delta E_{\text{kinetic}}$ and $\Delta E_{\text{Coulomb}}$, respectively) energy contributions to $\Delta E_{\text{total (Neutral)}}$. $\Delta E_{\text{total (Charged)}}$ is the result for $BaTiO_3$ doped at 0.15 e/(unit cell). All values are set to zero at Ti position = 0.50. (b) Contribution of kinetic ($\delta E_{\text{kinetic}}$) and Coulomb ($\delta E_{\text{Coulomb}}$) energy terms to the change in the deformation potential between charged and neutral states (δE_{total}).

B. Defect-induced phase transition

Next, we performed supercell calculations to clarify the role of the lattice disorder induced by donor dopants in doping-induced phase transitions. We considered Nb and oxygen vacancies as typical donor-type dopants. The range of dopant concentration was varied from $n_{\text{defect}} = 0.0185$ to 0.125 per unit cell by changing the supercell sizes (see Fig. 4). The accuracy of the k-point sampling grids is maintained as same as $8 \times 8 \times 8$ for unit cell, which enables us to compare the effects of dopant-induced lattice disorder and electron doping on the ferroelectric displacement of $BaTiO_3$ shown in Fig. 1. We also confirmed that reduction of the k-point grids down to the accuracy of $6 \times 6 \times 6$ have little influence on the obtained results, which suggest the strong influence of the lattice disorder induced by dopants in the supercell.

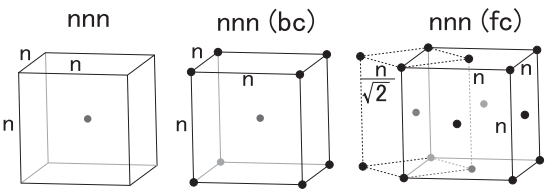

Supercell	Atom Number	Concentration /(unit cell)
222	39	0.1250
444 (fc)	79 (primitive)	0.0625
333	134	0.0370
444 (bc)	159 (primitive)	0.0313
666 (fc)	269 (primitive)	0.0185

FIG. 4. Supercell models composed of $n \times n \times n$ $BaTiO_3$ unit cells used the defect calculations. The notations bc (body center) and fc (face center) denote the defect positions within the supercells. Primitive cells are adopted in the calculations with fc and bc supercells.

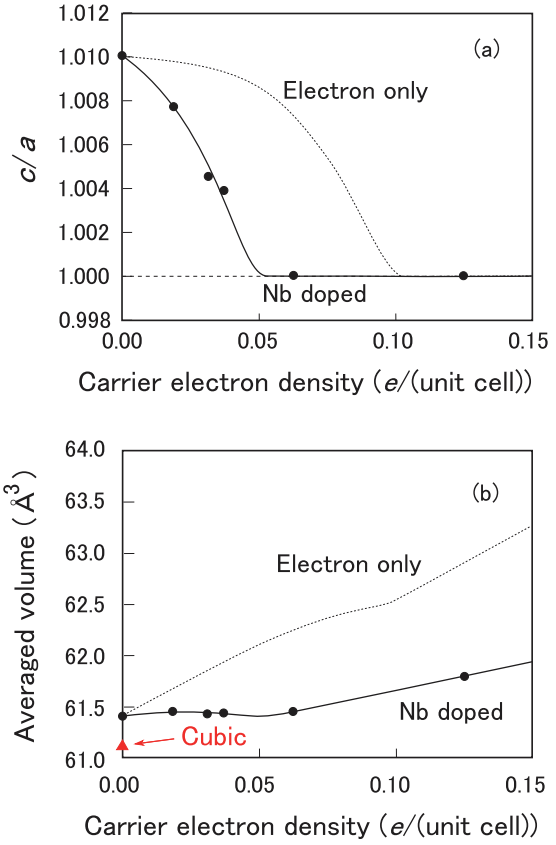

FIG. 5. (Color online) (a) The c/a ratio of Nb-doped supercells. (b) Average volume obtained by dividing supercell volume by the number of unit cells within the supercell.

Generally, Nb is considered to be Nb^{5+} occupying a Ti^{4+} site so that the number of carrier electrons is equal to the concentration of doped Nb^{5+}.[3,5] We confirmed that the band structure of an Nb-doped supercell agrees with this commonly accepted viewpoint. The change in the c/a ratio induced by Nb^{5+} doping is shown in Fig. 5(a), where the c/a ratio decreases faster than that in the electron-only calculation. The critical concentration of electrons for doping with Nb^{5+} is $n_{Nb} \approx 0.05$ e/(unit cell) (8.1×10^{20} cm^{-3}), which is about half the concentration found by the electron-only calculation. The larger ionic radius of Nb^{5+} compared with that of Ti^{4+} is responsible for the rapid reduction of the c/a ratio. The situation is confirmed by the smaller local c/a ratio around the Nb^{5+} dopant shown at position A in Fig. 6. Changes in

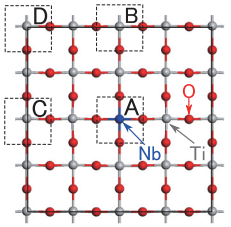

Position	c/a	Volume(Å^3)
A	1.002	61.92
B	1.007	61.29
C	1.003	61.34
D	1.005	61.19

FIG. 6. (Color online) c/a ratios and unit cell volumes at local positions A, B, C, and D in the cross-sectional view of the relaxed supercell that contains Nb^{5+}. The supercell size is 444 (bc), which corresponds to a Nb^{5+} concentration of 0.031 per unit cell.

the average volume obtained by dividing the supercell volume by the number of unit cells within the supercell are shown in Fig. 5(b). One unexpected finding is that the average volume of the Nb-doped supercell increases slower than that found by the electron-only calculation, despite the large ionic radius of the incorporated Nb^{5+} dopant. This result can be understood from the change in local unit cell volumes (see Fig. 6). Although the local unit cell volume around the Nb^{5+} impurity is sufficiently large (61.92 Å^3 at position A), local volumes far from Nb^{5+} (61.19 Å^3 at position D) are even smaller than the calculated volume for perfect tetragonal $BaTiO_3$ (61.40 Å^3). The decrease in the local volumes far from Nb^{5+} impurities causes the suppression of the supercell volume. As is well known from experiments, the thermal expansion coefficient of $BaTiO_3$ decreases sharply at each phase transition temperature from lower- to higher-symmetry phases,[16] which indicates that the volumes of the higher-temperature phases are intrinsically smaller than those of the lower-temperature phases at least near phase transition temperatures. In our calculations, the unit cell volume of C phase is smaller than that of T phase, as plotted in Fig. 5(b), reflecting the nature of $BaTiO_3$. Therefore, the average volumes tend to become smaller when the phase transition to C phase becomes more sensitive to the concentration of doped electrons. These results agree well with previous experiments with $BaTi_{0.875}Nb_{0.125}O_3$ (BTNO),[5] where the crystal structure is cubic ($Pm3m$) at room temperature with a small expansion of the cell parameter and the cubic phase remains down to 15 K.

We further calculated the effects of oxygen vacancies on the T-C phase transition in $BaTiO_3$. We confirmed that no in gap states from oxygen vacancies exist, which indicates that the vacancies are in a doubly charged state (V_O^{2+}).[27] These results are also consistent with recent theoretical studies using more accurate hybrid functional calculations.[28] Therefore, we assume here that two electrons are released from a V_O^{2+} vacancy, although much debate remains about the valence states of oxygen vacancies in perovskite-type oxides.[28–31] The inset of Fig. 7(a) shows the changes in tetragonality induced by V_O^{2+} types I and II, where types I and II indicate the two different positions of V_O^{2+} in T phase $BaTiO_3$ and are denoted by O_I and O_{II} in Fig. 1(a), respectively. Note that the two adjacent Ti atoms around V_O^{2+} move away from each other, as shown in Fig. 8. The lattice of the supercell is elongated in the direction of the shift of the two Ti atoms; hence, the c/a ratio for V_O^{2+} type I does not decrease monotonically but begins to increase around carrier electron concentrations greater than 0.06 e/(unit cell), as shown in the inset of Fig. 7(a). In contrast, for V_O^{2+} type II, the c/a ratio becomes less than 1 at the same carrier concentration, which means that the a axis replaces c axis as the longest axis because of the strong lattice disorder around V_O^{2+}. V_O^{2+} type I vacancy is slightly more stable than V_O^{2+} type II vacancy, but the difference between the total energy of the two oxygen vacancies is about two orders of magnitude smaller than the calculated oxygen vacancy formation energies (6.3−5.3 eV, depending on the supercell size of 39−259 atoms). Therefore, we can appropriately approximate the uniform distribution of V_O^{2+} type I and II vacancies in T phase $BaTiO_3$. We used a simple average of the c/a ratio to approximate the uniform distribution of two types of oxygen vacancies:

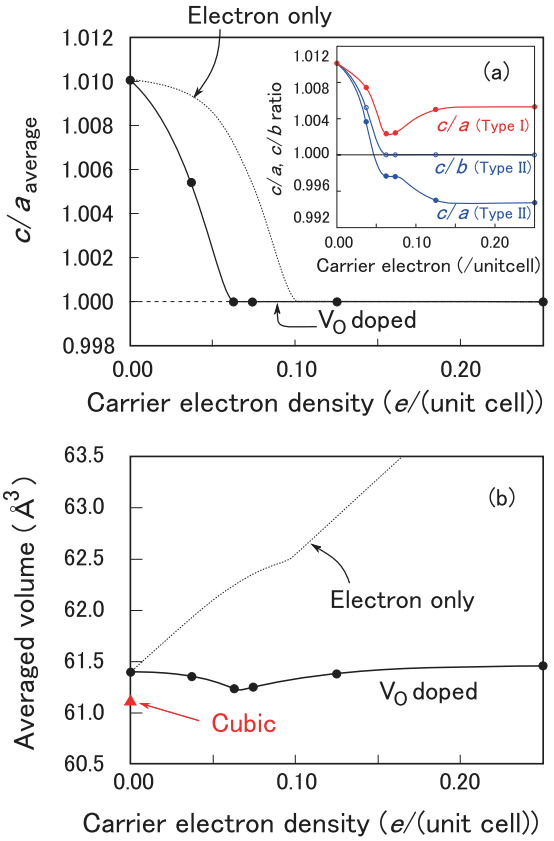

FIG. 7. (Color online) (a) The c/a ratio and (b) average volume calculated for V_O^{2+}-doped $BaTiO_3$ supercells.

$c/a_{\text{average}} = (c/a_{\text{type I}} + c/a_{\text{type II}} + c/b_{\text{type II}})/3$. The average tetragonality c/a_{average} is shown in Fig. 7(a). Tetragonal distortion disappears at the critical electron concentration of 0.06 e/(unit cell) (9.8×10^{20} cm^{-3}) and the T phases cannot be maintained if the V_O^{2+} concentration is increased further. The average unit cell volume remains almost constant independent of the V_O^{2+} concentration, as shown in Fig. 7(b). Although the local unit cell volume around V_O^{2+} increases significantly, as shown at position E in Fig. 8, decreases in volume at other areas far from the vacancies counteract this increase so that the average volume does not increase. Because the C phase occupies less volume than the T phase, a sharp decrease in volume at the phase transition point is a sign of T-C phase transition.

The Nb^{5+}- and V_O^{2+}-doped supercell calculations show that the dopant-induced lattice disorder reduces the critical carrier

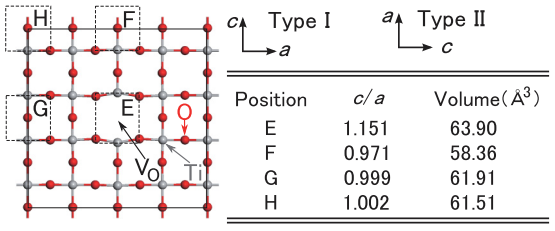

Position	c/a	Volume(Å^3)
E	1.151	63.90
F	0.971	58.36
G	0.999	61.91
H	1.002	61.51

FIG. 8. (Color online) c/a ratios and unit cell volumes at different local positions E, F, G, and H in the relaxed structure of 444 (bc) supercell with V_O^{2+} type I vacancy.

electron concentration where the T phase vanishes in $BaTiO_3$. Although the critical carrier electron concentrations in $BaTiO_3$ doped with Nb^{5+} and V_O^{2+} are very similar [0.05 and 0.06 e/(unit cell), respectively], the concentration of V_O^{2+} for the phase transition (0.03 per unit cell) is much smaller than that of Nb^{5+} (0.05 per unit cell). The oxygen vacancy strongly perturbs the $BaTiO_3$ lattice, as shown in Fig. 8, which causes phase transition at a lower concentration of oxygen vacancies compared with Nb^{5+} substitution.

The calculated critical electron density for the V_O^{2+} supercell is 0.06 e/(unit cell) (9.8×10^{20} cm^{-3}), which is about half the experimental value for reduced $BaTiO_{3-\delta}$ (1.9×10^{21} cm^{-3}).[1] We should carefully reconsider the difference between these results: The experimental value was obtained from changes in phase transition temperature caused by oxygen vacancy doping. The electron concentration where all ferroelectric phases disappear should be the critical electron density. However, because of the irreversible transformation into hexagonal polymorph caused by V_O,[1] experiments with heavily reduced $BaTiO_{3-\delta}$ are difficult. Hence, the critical electron density has to be evaluated from a linear extrapolation of the C-T transition temperature around electron concentrations of 1.0 to 3.5×10^{20} cm^{-3} from Ref. 1. However, there is no guarantee that the phase transition temperature decreases in proportion to electron concentration over such a wide range of electron doping. The disappearance of the ferroelectric distortion shown in Fig. 1 is definitely not proportional to electron concentration, which suggests that more higher-order fitting is required to evaluate the critical density. The critical density thus obtained is expected to be smaller than the reported experimental value.

In our calculations we treated the phase transition of $BaTiO_3$ as displacive; that is, all Ti ions are displaced along the [001] direction in the T phase ($P4mm$) and the C phase is microscopically nonpolar ($Pm3m$). However, the coexistence of displacive and order-disorder (microscopically polar) components in the C-T phase transition of $BaTiO_3$ has been pointed out both theoretically[32] and experimentally.[33] The C phase contains randomly [111]-oriented Ti ions in each perovskite lattice with no long-range order, which would be intrinsic to the phase transition in $BaTiO_3$ around the C-T phase transition temperature. However, the electron-induced phase transition is different; it can occur even at 0 K,[1] and our calculation for the R phase indicates that the local [111] atomic displacement vanishes as a result of electron doping. Therefore, we expect that the [111] atomic displacement from cubic symmetry is suppressed in the C phase achieved by electron doping at 0 K, which is a characteristic of the electron-induced phase transition of $BaTiO_3$. To the best of our knowledge, the detailed low-temperature behavior of the electron-induced phase transition remains unclear. To clarify the nature of carrier-electron-induced phase transitions in $BaTiO_3$, knowledge of the low-temperature structure of the electron-doped C phase near 0 K would be required.

IV. CONCLUSION

In conclusion, from first-principles calculation, the effect of electron doping on the disappearance of the ferroelectric phase was evaluated, namely the low- to high-symmetry

phase transition in $BaTiO_3$. Our calculations indicate that the disappearance of the ferroelectric phase is intrinsic to the nature of electron doping in $BaTiO_3$. The critical electron concentration for the T-C phase transition is calculated to be $n_{\text{elec.}} = 0.085\ e/(\text{unit cell})(1.36 \times 10^{21}\ \text{cm}^{-3})$. Component analysis of the total energy indicates that the screening of the Coulomb energy by carrier electrons is a main factor behind the disappearance of the ferroelectric lattice instability. In addition, we performed supercell calculations with donor dopants Nb^{5+} and V_O^{2+} explicitly introduced into the supercell models and clarified that dopant-induced lattice disorder accelerates the disappearance of the ferroelectric distortion in $BaTiO_3$. The critical electron concentration for T-C phase transitions upon doping with Nb^{5+} and V_O^{2+} is reduced to about one-half of the electron concentration for phase transitions induced by electron-only doping. In particular, the calculated critical electron density for the V_O^{2+} supercell model is 0.06 $e/$(unit cell) (9.8×10^{20} cm^{-3}), which is about half the experimental value.[1] This result suggests that more detailed research is necessary, including an experimental procedure to determine the critical electron density.

ACKNOWLEDGMENTS

The numerical calculations were partially carried out on TSUBAME2.0 at Global Scientific Information and Computing Center of Tokyo Institute of Technology supported by the MEXT Open Advanced Research Facilities Initiative. We thank Y. Gohda for many stimulating discussions. We also thank anonymous referees for their useful suggestions.

*y-iwazaki@jty.yuden.co.jp

[1] T. Kolodiazhnyi, M. Tachibana, H. Kawaji, J. Hwang, and E. Takayama-Muromachi, Phys. Rev. Lett. **104**, 147602 (2010).
[2] J. Hwang, T. Kolodiazhnyi, J. Yang, and M. Couillard, Phys. Rev. B **82**, 214109 (2010).
[3] J. F. Marucco, M. Ocio, A. Forget, and D. Colson, J. Alloys Compd. **262**, 454 (1997).
[4] V. Fritsch, J. Hemberger, M. Brando, A. Engelmayer, S. Horn, M. Klemm, G. Knebel, F. Lichtenberg, P. Mandal, F. Mayr, M. Nicklas, and A. Loidl, Phys. Rev. B **64**, 045113 (2001).
[5] K. Page, T. Kolodiazhnyi, T. Proffen, A. K. Cheetham, and R. Seshadri, Phys. Rev. Lett. **101**, 205502 (2008).
[6] O. Dieguez, S. Tinte, A. Antons, C. Bungaro, J. B. Neaton, K. M. Rabe, and D. Vanderbilt, Phys. Rev. B **69**, 212101 (2004).
[7] J. Iniguez and D. Vanderbilt, Phys. Rev. Lett. **89**, 115503 (2002).
[8] K. J. Choi, M. Biegalski, Y. L. Li, A. Sharan, J. Schubert, R. Uecker, P. Reiche, Y. B. Chen, X. Q. Pan, V. Gopalan, L.-Q. Chen, D. G. Schlom, and C. B. Eom, Science **306**, 1005 (2004).
[9] J. Junquera and P. Ghosez, Nature (London) **422**, 506 (2003).
[10] V. Petkov, V. Buscaglia, M. T. Buscaglia, Z. Zhao, and Y. Ren, Phys. Rev. B **78**, 054107 (2008).
[11] W. Y. Shih, W.-H. Shih, and I. A. Aksay, Phys. Rev. B **50**, 15575 (1994).
[12] T.-C. Huang, M.-T. Wang, H.-S. Sheu, and W.-F. Hsieh, J. Phys.: Condens. Matter **19**, 476212 (2007).
[13] T. Kolodiazhnyi, Phys. Rev. B **78**, 045107 (2008).
[14] R. E. Cohen, Nature (London) **358**, 136 (1992).
[15] R. E. Cohen, J. Phys. Chem. Solids **61**, 139 (2000).
[16] K. H. Hardtl and R. Wernicke, Solid. State. Commun. **10**, 153 (1972).
[17] M. D. Segall, P. J. D. Lindan, M. J. Probert, C. J. Pickard, P. J. Hasnip, S. J. Clark, and M. C. Payne, J. Phys.: Condens. Matter **14**, 2717 (2002).
[18] W. A. Al-Saidi and A. M. Rappe, Phys. Rev. B **82**, 155304 (2010).
[19] R. Wahl, D. Vogtenhuber, and G. Kresse, Phys. Rev. B **78**, 104116 (2008).
[20] A. Filippetti and N. A. Hill, Phys. Rev. B **65**, 195120 (2002).
[21] Y. Xie, H.-t. Yu, G.-x Zhang, and H.-g. Fu, J. Phys.: Condens. Matter **20**, 215215 (2008).
[22] D. J. Singh, M. Ghita, M. Fornari, and S. V. Halilov, Ferroelectrics **338**, 73 (2006).
[23] M. Ghita, M. Fornari, D. J. Singh, and S. V. Halilov, Phys. Rev. B **72**, 054114 (2005).
[24] K. Uchida, S. Tsuneyuki, and T. Schimizu, Phys. Rev. B **68**, 174107 (2003).
[25] W. Zhong and D. Vanderbilt, Phys. Rev. Lett. **74**, 2587 (1995).
[26] The analysis of the total energy is performed by using Tokyo *ab initio* program packages (TAPP); J. Yamauchi, M. Tsukada, S. Watanabe, and O. Sugino, Phys. Rev. B **54**, 5586 (1996).
[27] W. Luo, W. Duan, S. G. Louie, and M. L. Cohen, Phys. Rev. B **70**, 214109 (2004).
[28] M. Choi, F. Oba, and I. Tanaka, Appl. Phys. Lett. **98**, 172901 (2011).
[29] J. Carrasco, F. Illas, N. Lopez, E. A. Kotomin, Yu. F. Zhukovskii, R. A. Evarestov, Yu. A. Mastrikov, S. Piskunov, and J. Maier, Phys. Rev. B **73**, 064106 (2006).
[30] D. Ricci, G. Bano, G. Pacchioni, and F. Illas, Phys. Rev. B **68**, 224105 (2003).
[31] D. D. Cuong, B. Lee, K. M. Choi, H.-S. Ahn, S. Han, and J. Lee, Phys. Rev. Lett. **98**, 115503 (2007).
[32] W. Zhong, D. Vanderbilt, and K. M. Rabe, Phys. Rev. Lett. **73**, 1861 (1994); Phys. Rev. B **52**, 6301 (1995).
[33] E. A. Stern, Phys. Rev. Lett. **93**, 037601 (2004)